ACS Biomaterials SCIENCE & ENGINEERING
Cite This: ACS Biomater. Sci. Eng. 2019, 5, 2587−2594
Article
pubs.acs.org/journal/abseba

Enhanced Electrochemical Activity of a Hollow Carbon Sphere/Polyaniline-Based Electrochemical Biosensor for HBV DNA Marker Detection

Razieh Salimian,[†] Saeed Shahrokhian,*[,†,‡] and Saba Panahi[†]

[†]Department of Chemistry, Sharif University of Technology, Azadi Ave., Tehran 11155−9516, Iran
[‡]Institute for Nanoscience and Technology, Sharif University of Technology, Azadi Ave., Tehran 11155−9516, Iran

Supporting Information

ABSTRACT: Herein, we present a novel, simple, and ultrasensitive electrochemical DNA (E-DNA) sensor based on hollow carbon spheres (HCS) decorated with polyaniline (PANI). A thiolated 21-mer oligonucleotide, characteristic of HBV DNA, is immobilized via electrodeposited gold nanoparticles on HCS-PANI. Cyclic voltammetry (CV), differential pulse voltammetry (DPV), and electrochemical impedance spectroscopy (EIS) are used to characterize the electrochemical properties of the prepared nanocomposite. Scanning electron microscopy is employed to investigate the morphological texture of the fabricated modifier. An enhanced intrinsic signal of PANI is probed to evaluate the biosensing ability of the prepared modifier. The proposed biosensor allows for the detection of the target sequences of HBV DNA at a concentration as low as 10 fM (i.e., 10^9 DNA copies/mL). In addition, this biosensor demonstrated good capability to differentiate between the perfectly matched target oligonucleotide and three nucleotide-mismatched oligonucleotides. Furthermore, the HCS/PANI-based E-DNA sensor indicates highly sensitive detection of HBV DNA in real samples.

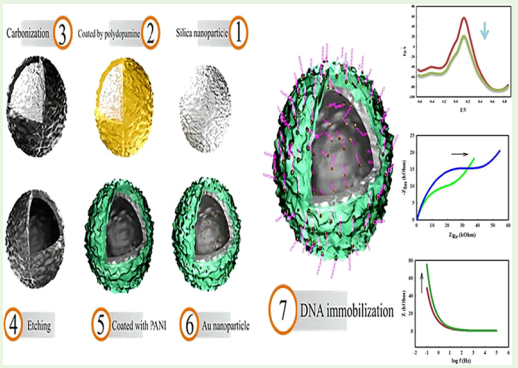

KEYWORDS: *hepatitis B virus, hollow carbon sphere, polyaniline, gold nanoparticle, self-redox signal, label-free detection, electrochemical biosensor*

INTRODUCTION

Hepatitis B virus (HBV), a serious infectious and widespread human pathogen, represents a vital health problem throughout the world. Chronic HBV infection, as a partially double-stranded DNA virus, has a very high risk of evolving into hepatocellular carcinoma (HCC).[1] This virus is widely spread through the blood and other body fluids. Many HBV markers have been identified and used in the diagnosis and monitoring of the disease and its progression. Among them, HBV DNA is a reliable marker of HBV activity and is detectable within a few days after infection. High levels of HBV DNA are associated with a higher incidence of HCC and more rapid progression to cirrhosis.[2] According to the National Center for Biotechnology Information (NCBI),[3] HBV DNA levels can vary from a few to more than 10^9 copies/mL in human serum, and they are usually detected for active infection in serum or blood samples.[4] As the number of infectious people increases, the demand for highly sensitive diagnostic devices soars. Among various analytical methods, electrochemical detection assays have the advantage of being simple, reliable, cheap, sensitive, and selective for genetic detection.[5,6]

Polyaniline (PANI), known as a π-conjugated organic polymer that features high conductivity, excellent biocompatibility, and controllable nanostructure, has attracted considerable attention and has shown a great potential application in the electrochemical biosensing field.[7,8] Despite all of these features, PANI reveals its conductivity and redox characteristics only in an acidic medium (pH < 4). Therefore, the loss of redox activity of PANI in neutral media precludes the coupling of this conducting polymer to a biological system and leads to poor selectivity, sensitivity, and detection limit in DNA sensors.[9] To overcome this limitation, a variety of approaches have been reported, including the functionalization of PANI with acidic functional groups,[10] doping it with negatively charged polymers,[11] and also, using metal nanoparticles[12] or carbon nanostructures.[13] Each of the proposed methods can expand the range of polymer applications from a neutral to the basic pH range. Among the proposed strategies, carbon nanostructures, due to their supreme electronic transport properties, extremely high mechanical strength, high specific surface area, and exceptional thermal conductivity, are a promising candidate to improve the merit of PANI in the biosensing field.[14]

Received: December 3, 2018
Accepted: March 21, 2019
Published: March 21, 2019

DOI: 10.1021/acsbiomaterials.8b01520
ACS Biomater. Sci. Eng. 2019, 5, 2587−2594

The diversity of carbonic structures does not end at the fullerene, carbon nanotubes, and graphene.[15,16] Nowadays, the fabrication of hollow and porous carbon nanostructures, produced via carbonization of organic materials, is extensively progressing. Well-defined pore structures, remarkably high surface areas, extremely short mass diffusion and transport resistance, and precisely tuned pore sizes are some highlighted features of hollow carbon structures.[17] Templating is the most straightforward way to synthesize hollow carbon spheres (HCSs). Typically, a carbon precursor is coated on a hard template core, as a shell. HCSs are obtained upon the carbonization and core removal.[18] In this regard, the carbon precursors play a key role in the physicochemical properties of the resulting carbon framework composition. Taking advantage of strong and versatile coating capability, dopamine, as a biomolecule that contains catechol and amine functional groups and can simply self-polymerize at alkaline media and spontaneously deposit on virtually any surface, shows excellent performances in the preparation of carbon-coating materials.[19]

Numerous works on a PANI-based electrochemical DNA sensor have been introduced in recent years. Daunomycin,[20] methylene blue,[21] hexacyanoferrate,[22] 3,3′,5,5′-tetramethylbenzidine (TMB),[23] ruthenium hexamine,[24] and 1-naphthyl phosphate[25] are some of the common indicators, which have been used for DNA detection on this polymeric structure. Using such a redox indicator in one independent step would impress the simplicity of the detection procedure, biosensor fabrication, and make these methods more laborious and time-consuming.

In the present work, a thin layer of PANI is synthesized on hollow carbon nanoparticles, which are used as an efficient modifier with an improved electron transfer rate and high surface area properties. This novel substrate satisfies the constraint of polymer application in neutral metrics. Eventually, the detection of the HBV DNA marker is performed by stabilizing the thiolated-probe DNA on gold nanoparticles (GNPs) decorated on HCS-PANI nanostructures, following the intrinsic redox peak of the PANI peak. A nanoporous layer is successfully used for the ultrasensitive detection of DNA in human plasma samples.

EXPERIMENTAL SECTION

Chemical and Reagents. Dopamine hydrochloride (DA) (Merck), tetraethylorthosilicate (TEOS) (99.0%, Sigma-Aldrich), 6-mercapto-1-hexanol (MCH) (Sigma-Aldrich), ethanol (Sigma-Aldrich), ammonium hydroxide (28.0%, Sigma-Aldrich), aniline (99.5%, Sigma-Aldrich), tris(2-carboxyethyl)phosphine (TCEP) (Sigma-Aldrich), potassium chloride (KCl) (Sigma-Aldrich), potassium nitrate (KNO_3) (Sigma-Aldrich), magnesium chloride ($MgCl_2$) (Sigma-Aldrich), ammonium persulfate (APS) (Sigma-Aldrich), potassium ferrocyanide ($K_4Fe(CN)_6$) (Merck), potassium ferricyanide ($K_3Fe(CN)_6$) (Merck), phosphoric acid (H_3PO_4) (Sigma-Aldrich), hydrochloric acid (HCl) (Sigma-Aldrich), sodium hydroxide (Merck), and human serum albumin (HSA) (Iranian Blood Transfusion Organization) were all used as received. Gold bullion (99.9%) was dissolved in Aqua Regia and diluted with 0.1 M HCl to form a gold stock solution (5 mM). Milli-Q water (18.2 MΩ cm^{-1}) was used throughout the experiments.

For our studies, we employed the following sequence as our electrochemical DNA (E-DNA) "probe", which was purchased from Bioneer (Daejeon, Korea) and ascribed as the HBV probe, 5′-OH-C_6-(S-S)-$(CH_2)_6$-GAG GAG TTG GGG GAG CAC ATT-3′. As the target oligonucleotides for this biosensor, the following unmodified DNA strands were used, complementary (Com), 5′-AAT GTG CTC CCC CAA CTC CTC-3′; noncomplementary (NC), 5′-AAC GTG TGA ATG ACC CAG TAC-3′; and mismatch target (MT) (3MT), 5′-AAT GTG GTC CCC GAA CTC GTC-3′.

Apparatus. All electrochemical measurements were carried out using a Potentiostat/Galvanostat (AUTOLAB 204N) and a Metrohm Unit 757 VA Computrace instruments (Metrohm, Herisau, Switzerland) system. A conventional three electrode configuration consists of a glassy carbon working electrode (GCE, 2.0 mm diameter), an Ag/AgCl/KCl (3.5M) reference electrode, and a Pt wire counter electrode was used for testing the DNA assay. The experimental solutions were degassed with nitrogen for at least 600 s prior to the electrochemical investigations. In the differential pulse voltammetry (DPV) method, the modulation amplitude was 50 mV, the step potential was 6 mV, and the apparent scan rate was 15 mV s^{-1}, in the range potential of −0.6 to 0.6 V.

Synthesis of HCSs. Typically, the synthesis of the polydopamine−silica (PDA-silica) composite is carried out using silica nanoparticles, produced from a known Stöber method,[26] as the template. In the subsequent step, self-polymerization of DA, as a carbon precursor, is performed under the basic condition.[19] Recently, Noonan and co-workers,[27] reported the production of silica-PDA composite nanospheres under the modified Stöber conditions. In this regard, by shortening the usual synthetic time, not only the possibility of simultaneous silica-PDA synthesis is provided, but also the improvement of the final production's structure in mesoporous format is achieved. Briefly, a solution containing EtOH, DI water, and NH_4OH was mixed under vigorous stirring. Then, 2.8 mL of TEOS was added dropwise. After 30 min, DA was added, and the mixture was stirred at room temperature for 12 h. The resulting dark brown precipitate was rinsed with water and ethanol and collected by centrifugation before drying overnight in a 60 °C oven. To convert the PDA to nitrogen-doped carbon, the silica-PDA composite powder was carbonized under an N_2 atmosphere at 800 °C for 5 h with a heating rate of 5 °C min^{-1}. After that, silica cores were removed by dispersing the composite particles in 1 M NaOH solutions at 30 °C for 24 h, followed by being centrifuged and dried at 60 °C. Finally, the obtained hollow carbon spheres were denoted as HCS.

Preparation of PANI-Coated HCS (HCS-PANI). The growth of PANI on the surface of HCSs was performed by the oxidative polymerization of aniline in the presence of HCSs, as previously reported in the literature by Zhao.[28] Typically, 30 mg of HCSs was dispersed in 20 mL of HCl aqueous solution (2.0 mol/L) under sonication for 10 min and was followed by the addition of a small portion of aniline (30 μL) while stirring gently. After being stirred for 30 min, ammonium persulfate, as an oxidizing agent, was added in two steps. In the first step, ammonium persulfate was added with a ratio of 1:4 (ammonium persulfate: aniline). After 30 min, the ratio was increased by 4:1, and the color of the mixture changed to dark green. The polymerization of aniline in the presence of HCS was allowed to proceed at room temperature (25 °C) for 12 h. The products were collected by repeatedly centrifuging and washing with deionized water and ethanol and dried in a 60 °C oven. The obtained HCS-PANI composite is supposed to form a uniform core−shell structure (HCS@PANI).

Electrode Modification and Sensor Fabrication. The electrode modification was carried out in two steps, including transferring the synthesized HCS-PANI on the electrode surface, followed by electrochemical deposition of GNP for trapping the DNA probe via Au−S bond formation. In brief, prior to sensor fabrication, glassy carbon electrodes (GCEs, Azar electrode, Urmia; diameter 2 mm) were cleaned both mechanically (by polishing on a fine-grain sandpaper (1200 grit) until a mirror-like finish was obtained) and electrochemically (by cycling in PBS for 10 scans in the potential range of −0.2 to 1.0 V (scan rate 0.1 V s^{-1}), until reproducible voltammograms were obtained). In the next step, a desired amount of HCS-PANI composite was casted on the surface of a GCE using ambient temperature for homogeneous drying, followed by drying in a 50 °C oven. Subsequently, electrochemical deposition of GNPs was performed at −0.2 V for 200 s by dipping the HCS-PANI/GCE in 0.1 M KNO_3 containing 1 mM $HAuCl_4$. The final electrode was named as Au/HCS-PANI/GCE.

DOI: 10.1021/acsbiomaterials.8b01520
ACS Biomater. Sci. Eng. 2019, 5, 2587−2594

E-DNA sensors were prepared by applying the following procedure. First, the linear DNA probes were reduced through incubation in freshly prepared 0.5 mM TCEP solution for 1 h, at room temperature in the dark. After that, the solution was diluted to a final concentration of 10 μM (PBS of pH = 7.0, containing 0.1 M $MgCl_2$). Then, 10 μL of the DNA probe was dropped on the surface of Au/HCS-PANI/GCE. After DNA immobilization, the electrode surface was backfilled with MCH (2 mM) for 30 min to remove, followed by being rinsed with ultrapure water and stored in buffer for future use.

RESULTS AND DISCUSSION

Structural Analysis of HCS and HCS-PANI via Infrared Spectroscopy. An FT-IR technique was used to investigate the chemical composition of the synthesized compounds. As shown in Figure 1A, the presence of Si is displaced with a strong peak expanded in a wide wavenumber range from 1020 to 1140 cm^{-1}, which is related to the asymmetric vibration of SiO_4, stretching vibrations of Si−OH groups, and the Si−O−Si symmetric tensile (spectrum a). The appearance of the characteristic peaks of dopamine, including 1206 cm^{-1} for C−O and 1581 and 1491 cm^{-1} for the resonance vibration of C−C in the ring of benzene and scissor vibration of N−H, confirms the stabilization of PDA on the surface of SiO_2 nanospheres (spectrum a). Also, overlapping of the characteristic peaks of SiO_2 nanoparticles and PDA are observed in this spectrum. Subsequently, by the carbonization of the polymeric structure and removal of SiO_2 (Figure 1A,b), most of the characteristic bands of organic groups are disappeared, confirming that the PDA groups are successfully carbonized. Also, disappearance of the band in 1100 cm^{-1} suggests successful removal of SiO_2 from the structure. Finally, after the polymerization of aniline, the structural peaks of PANI are shown in Figure 1A,c. The bands at 1133, 1298, 1493, and 1571 cm^{-1} are related to the stretching vibrations of N═Q═N (Q is quinoneoid ring), stretching vibration of C−N, and stretching vibration (C═C) of the benzoyl and the quinoneide rings.[29]

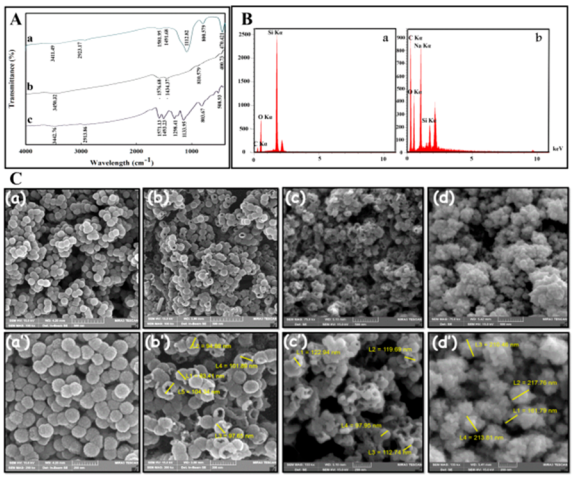

Figure 1. (A) The FT-IR spectrum of (a) PDA-coated SiO_2 nanoparticles (SiO_2@PDA), (b) HCS, and (c) HCS-PANI. (B) EDX spectrum of (a) SiO_2@PDA and (b) HCS. (C) SEM of (a) SiO_2@C, (b) HCS, (c) HCS-PANI, and (d) Au/HCS-PANI, in two different magnifications of (a, b, c, d) 500 and (a′, b′, c′, d′) 200 nm.

Morphological Characterizations of HCS and HCS-PANI using Scanning Electron Microscopy (SEM). The morphological structure of various synthesized samples was studied using scanning electron microscopy (SEM). The morphology of the carbonic framework before and after dissolution of the silica template is displayed in Figure 1C. As expected, all globes exhibit an uniform spherical morphology similar to the primary silica core with a particle diameter of about 100 nm (Figure 1C,a). After removing the silica template, the hollow character of HCS is clearly manifested by the presence of open windows on the external surface of HCS (Figure 1C,b). The agglomeration of these HCSs occurred through the strong bonding of the neighboring nanoparticles during the polymerization of dopamine. The thickness of this carbonic layer is estimated to be between 20 and 30 nm. In the presence of PANI (Figure 1C,c), the morphology of the HCS-PANI compounds is approximately the same as the HCS structures, only the outer surface becomes rougher. All the carbon beads are completely covered by a thin layer of PANI and form a core−shell structure (HCS@PANI). This layer has a thickness of about 20 nm, and most windows are wrapped up with this polymeric shell. After the electrodeposition of GNPs on the surface of the HCS-PANI nanocomposite, a rock-shaped GNP forms on the surface of these spherical structures, which produces a thickness of about 90 nm (Figure 1C,d). At each stage of the deposition, a surface coating with a high surface area is created for further deposition and eventually for immobilization of a biological layer. The excellent removal of SiO_2 can also be proven based on the energy-dispersive X-ray (EDX) spectrum in Figure 1B. As can be seen, after the carbonization and dissolution of Si (Figure 1B,b), the percentage of Si is significantly reduced, and the percentage of C is remarkably increased.

Electrochemical Properties of Modified Electrodes HCS, HCS-PANI, Au/HCS-PANI. Cyclic voltammetry (CV) and electrochemical impedance spectroscopy (EIS) techniques were used to investigate the electrical features of the modified electrodes. Initially, the microscopic surface area of bare GCEs as well as GCEs modified with the synthesized nanostructures, including HCS, HCS-PANI, and Au/HCS-PANI, was calculated using the CV at different scan rates of potential in 0.1 M KCl solution containing an 1 mM $[Fe(CN)_6]^{3-/4-}$ redox probe. As shown in Figure 2A, by modification of the electrode surface with a synthesized material at different stages, the observed current increases significantly, which can be related to the intrinsic properties of these nanostructures, including high conductivity and high surface area.

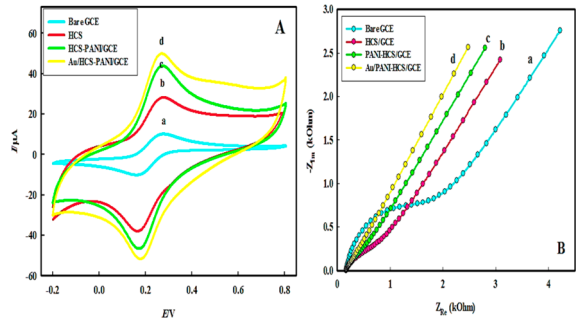

Figure 2. (A) CVs and (B) Nyquist plots of (a) GCE, (b) HCS/GCE, (c) HCS-PANI/GCE, and (d) Au/HCS-PANI/GC in 0.1 M KCl containing 1 mM $[Fe(CN)_6]^{3-/4-}$. Scan rate was 0.1 V s^{-1}, and the frequency range was between 100 kHz and 10 mHz.

DOI: 10.1021/acsbiomaterials.8b01520
ACS Biomater. Sci. Eng. 2019, 5, 2587−2594

For a reversible electrode process, the Randles-Sevcik eq (eq 1) is used to compute the active microscopic surface area of the mentioned modified electrodes

$$I_{p,a} = (2.69 \times 10^5)(n^{3/2})AC_oD^{1/2}\upsilon^{1/2} \quad (1)$$

where $I_{p,a}$ is the equivalent peak current, n is the number of the transferred electrons, A is the active electrode surface area, D is the diffusion coefficient, C_o is the concentration of redox species, and υ is the scan rate. The microscopic area of the electrode surface is obtained from the slope of $I_{p,a}$ versus $\upsilon^{1/2}$ graph (considering n = 1 and D = 7.6 × 10^{-6} cm^2/s). The results show a multiplier increase in the surface area of the modified electrode relative to the bare electrode (Table S1).

On the other hand, EIS was used for the investigation of the interfacial properties of the electrode/electrolyte. Figure 2B illustrates the Nyquist plot of 1 mM $[Fe(CN)_6]^{3-/4-}$ at the surface of four different electrodes. In the Nyquist diagram, the low-frequency region is associated with the mass transfer limitations (Warburg impedance), and the high-frequency region is related to the kinetic resistance of the electrochemical reaction at the electrode/electrolyte interface. As can be seen, a semicircle with relatively large diameter is observed at the surface of the GCE. With further modification of the electrode surface with the synthesized nanostructures, including HCS, HCS-PANI, and Au/HCS-PANI, the corresponding semicircular diameters are reduced, respectively. The results show an enhanced electrode kinetics at the surface of the modified electrodes.

Electrochemical Behavior of Various Modified Electrodes in Phosphate Buffer Solution. The inherent properties of PANI, such as doping and its oxidation level, will certainly affect its electrochemical properties. As mentioned earlier, the use of carbon structures is a promising way to modify PANI for use in a neutral media. For carbonic samples covered with PANI, as shown in Figure 3, a wide pair

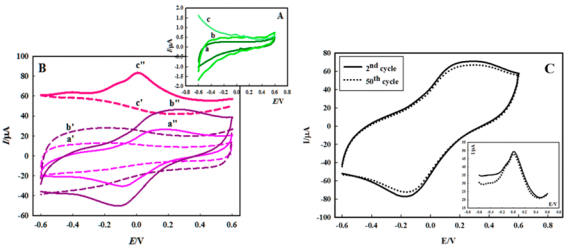

Figure 3. (A) GCE (a, b, c) (B) HCS/GCE (a′, b′, c′), and HCS-PANI/GCE (a″, b″, c″). (a) CVs at the scan rate of 0.05 V s^{-1}, (b) CVs at the scan rate of 0.1 V s^{-1}, and (c) differential pulse voltammograms. (C) Voltammograms of the stability test of the HCS-PANI-modified GC electrode with a 0.05 M phosphate buffer solution. Scan rate was 0.1 V s^{-1}.

of redox peaks arises from overlapping two redox processes, and those obtained in acidic conditions (Figure 3B,a″,b″,c″)[30] are observed. The CVs for the naked-GCE (Figure 3A,a,b,c) and the modified electrode with HCS (3B,a′,b′,c′) are also presented. The results clearly show that, with this modification, the conducting polymer can maintain its redox activity in neutral matrices. In addition, the electrochemical response of PANI maintains its repeatability and sustainability through multiple potential cycles (Figure 3C). This excellent stability of the PANI film in the neutral pH range is a basic requirement for its practical application in electrochemical biosensing and bioengineering applications.

In the next step, the effect of the potential scan rate (in the range of 25−350 mV s^{-1}) on the voltammetric behavior of the prepared modified electrodes was assayed. The corresponding voltammograms at the surface of HCS-PANI/GCE and Au/HCS-PANI/GCE (in phosphate buffer solution of pH 7.0) are shown in Figure S1A,B, respectively. As can be seen, PANI exhibits its electroactive characteristic by displaying its redox peak in the range of −0.6 to 0.6 V. The linear correlation between the logarithmic curve of the anodic and cathodic peak currents versus the logarithm of the scan rate with a slope equal to 0.5 indicates a diffusion-controlled process (ion movement into/from the solution from/into the modifier film). Also, a relatively fast charge transfer process at the interface of the polymer-modified electrode with electrolyte solution can be concluded.

After the electrodeposition of gold nanostructures on the surface of HCS-PANI/GCE, the prepared electrode was subjected to a similar test to examine the changes in the peak currents. As it is shown in Figure S1C,D, by deposition of AuNPs, the current increases. Thus, it can be concluded, that the surface area is increased, the rate of electron transfer is improved, and the ion penetration toward the surface is facilitated. As a result, these GNPs with a high surface area provide a suitable platform for the immobilization of ssDNA.

Analysis of DNA/Au/HCS-PANI/GC Electrode in Phosphate Buffer Solution. The electrochemical behavior of the modified electrode in the presence of the ssDNA probe strand was investigated. As is shown in Figure S2, in the presence of negatively charged biomolecules, which make a barrier against the ion penetration and electron transfer reaction for electroactive substances with similar charges, the current is decreased.

Optimization of Effective Parameters on Hybridization. The effects of some important experimental factors, such as temperature and incubation time, on the response characteristics of the fabricated biosensor were investigated. The incubator temperature is one of the most important parameters, which can impress the interaction of two strands of DNA. Exposing the biosensor to an inappropriate temperature can result in an incomplete interaction or destruction of DNA strands. The effect of incubation temperature on the current difference (compared to the control current) was studied between 25 and 65 °C. As shown in Figure S3A, after being incubated with a 10 pM target and increasing the temperature, the current response of the biosensor is enhanced (ΔI increases). However, by increasing the temperature higher than 45 °C, the current response is decreased (ΔI decreases), which means that increasing the temperature to 45 °C has a positive effect on the biosensor response. It is possible that the DNA structure on the electrode is damaged at higher temperatures. Therefore, a temperature of 45 °C was chosen as the optimum value for further studies.

On the other hand, since the interaction of the target sequences with the surface DNA probes is a time-consuming process, finding the optimal time has a considerable effect on the response sensitivity of the biosensor. As a result, the biosensor was placed in a 10 pM solution of the HBV DNA complementary target for various times from 10 to 60 min. As shown in Figure S3B, the difference of the electrochemical current response increases up to 40 min and eventually reaches a constant level, indicating the surface saturation of the

DOI: 10.1021/acsbiomaterials.8b01520
ACS Biomater. Sci. Eng. 2019, 5, 2587−2594

modified electrode at this time. Therefore, 40 min was selected as the optimal incubation time for the appropriate interaction of the surface-confined DNA and the HBV DNA target.

Analytical Investigation of DNA/Au/HCS-PANI/GCE in $[Fe(CN)_6]^{3-/4-}$ Solution. The response of the modified electrode was evaluated using $[Fe(CN)_6]^{3-/4-}$ as an external standard probe for monitoring the presence of the probe DNA and its subsequent interaction with the target DNA, under the optimum condition. As shown in Figure 4A, due to the

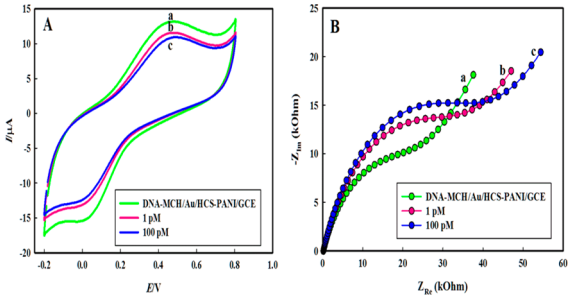

Figure 4. (A) CVs and (B) Nyquist diagrams of Au/HCS-PANI/GCE in the presence of (a) ssDNA and in the presence of complementary strands with a concentration of (b) 1 and (c) 100 pM, in 0.1 M KCl containing 1 mM $[Fe(CN)_6]^{3-/4-}$. Frequency range was between 100 kHz and 10 mHz.

presence of the polyanionic macromolecule (DNA), the anionic redox probe is effectively repelled from the surface of the electrode. The rate of the electron transfer is lowered, and a significant displacement of the redox peak potential is observed. In the following, the current response continues to decrease with increasing the concentration of HBV DNA from 1 to 100 pM complementary strand. Increasing the amount of R_{ct} during various stages of the surface modification with DNA proves that ssDNA probes have been successfully immobilized and then hybridized at the surface of the modified electrode (Figure 4B). Values for R_{ct} and R_s are listed in Table S2.

Performance of Biosensor in Detection of Various Concentrations of HBV. To evaluate the practical applicability of the proposed method, the Au/HCS-PANI-modified electrode was subjected to different concentrations of complementary HBV under the optimum conditions. The oxidation peak current versus HBV DNA concentration is plotted in Figure 5. The obtained peak currents are reduced by increasing the concentration of the complementary HBV strands. As a result, the DPV peak current of PANI shows a

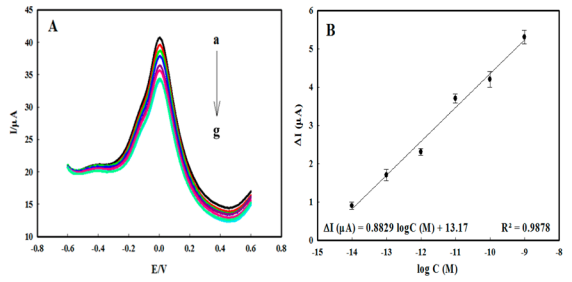

Figure 5. (A) Background-subtracted differential pulse voltammograms of biosensor after exposure to different concentrations of HBV from 0.01 pM to 1 nM (from a to g, a is a control sample). (B) The corresponding calibration curve of the current difference (ΔI) versus the logarithm of the concentration.

linear relationship (eq 2) with the logarithmic concentration of HBV in the range of 10 fM to 1 nM, with a detection limit of 3.62 fM (in terms of S/N = 3). The biocompatibility of this modifier can be attributed to two main factors. (1) The Au/HCS-PANI modifier not only provides a favorable environment for maintaining the activity of the biofilm but also increases the capacity of loading DNA probes on the electrode surface, due to providing a high surface area for the biosensor. (2) The Au/HCS-PANI modifier on the electrode surface provides a thin film with relatively high electrochemical activity.

$$\Delta I = 0.8829 \log C\ (\mathrm{M}) + 13.17\ (R^2 = 0.9878) \qquad (2)$$

The hybridization process and alternation of the electrochemical parameters can also be considered from another perspective. Since PANI on the surface of the hollow carbon nanoparticles can maintain its electrochemical activity in the phosphate buffer, changes in the interfacial properties between the modified electrode and electrolyte were investigated using the EIS technique in the buffer solution. As shown in Figure 6A, the HCS-PANI nanocomposite exhibits very little charge

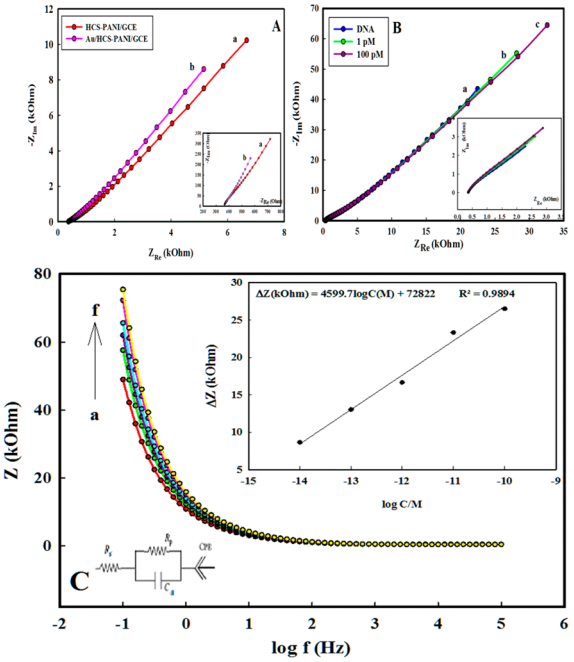

Figure 6. Nyquist plots of (A) (a) HCS-PANI and (b) Au/HCS-PANI. (B) Nyquist plots of Au/HCS-PANI/GCE in the presence of (a) ssDNA at (b) 1 and (c) 100 pM of the complementary HBV strand. (C) Bode plots of Au/HCS-PANI (a) ssDNA and various concentrations of (b) 0.01, (c) 0.1, (d) 1, (e) 10, and (f) 100 pM of the complementary HBV strand. (Inset) Corresponding calibration curve and equivalent circuit in the frequency range between 100 kHz and 100 mHz.

transfer resistance (R_{ct}), which is lowered in the presence of GNPs. This is good evidence for fast kinetics of electron transfer in the presence of metallic nanomaterials. On the other hand, increasing the slope of the linear part of this diagram (Figure 6A) in the Au/HCS-PANI sample (a) compared to HCS-PANI (b) refers to facilitating the penetration of ions into the structure and highlights a remarkable role of GNPs in reducing the mass transfer resistance for ion diffusion. Subsequently, in the presence of the DNA probe and HBV

DOI: 10.1021/acsbiomaterials.8b01520
ACS Biomater. Sci. Eng. 2019, 5, 2587−2594

Table 1. Comparison of the Characteristics of the Proposed Electrochemical Biosensors for Detection of HBV DNA

electrode	technique	redox species	linear range	LOD
GNR/GE[34]	CV	$[Co(phen)_3]^{3+}$	1 pM−1 μM	2 pM
GQD/GCE[35]	DPV	$[Fe(CN)_6]^{3-/4-}$	10−500 nM	1 nM
paper electrochemical sensor[36]	ASV	Ag NPs	1 pM−1.5 nM	85 pM
MNP/GNP/CPE[37]	EIS	MB	1 pM−10 nM	0.31 pM
hemin/G-quadruplex DNAzyme[38]/GE	DPV	TMB	10 pM−10 nM	0.5 pM
PABA/GCE[39]	DPV	Au NPs host−guest recognition	0.4 pM−4 nM	0.3 pM
GE[40]	ACV	MB-DNA	1 fM−1 nM	5 fM
CHIT-CNF-PGE[41]	DPV	guanine oxidation	16−3.2 μM	1.74 μM
GE[42]	DPV	GON-Ag NPs	10 fM−10 nM	7.6 fM
GE[43]	DPV	MB RCA	10−700 aM	2.6 aM
SWCNT/GNP[44]	EIS	$[Fe(CN)_6]^{3-/4-}$	1 aM−1 μM	1 aM
GE[45]	CA	RuHex	100 pM−0.1 μM	100 pM
PICA−MWNT/GCE[46]	CV	PICA	10 fM−5 pM	2 fM
Au NRs-GO/GCE[47]	DPV	MB	10 fM−1 nM	3.5 fM
Au/HCS-PANI/GCE (this work)	DPV	PANI	0.01 pM−1 nM	3.62 fM

DNA target with different concentrations (Figure 6B), the charge transfer resistance on this film is slightly increased. In addition, in the mass transfer region of the Nyquist plot (considering the effect of the two factors, including slope and frequency range for the Warburg region), the slope of the line is gradually decreased (toward the Z_{Re} axis) due to prevention of ion diffusion on the modified electrode surface. These results can be considered as a good reason for reducing the current, as shown in Figure 5.[31]

For a better clarification, a Bode plot, in which the absolute value of Z was depicted against the logarithm of frequency in the range of 100 kHz to 0.1 Hz, is shown in Figure 6C. During the addition of a target HBV DNA, the impedance value of Z shows the maximum change at a frequency less than 1 Hz. This effect can be explained by the equivalent circuit defined for the above system (Figure 6C, inset). In this circuit, R_s represents the electrolyte resistance, the internal resistance of the electrode, and the resistance of all connections and wires. R_p represents the electron transfer resistance of the modifier layer, and C_p represents the capacitance for the double-layer formed at the electrode surface. At very high frequencies, where the double-layer capacitance of the electrode surface is not substantially charged, the capacitance associated C_p is very small, and all curves have impedance values close to R_s. When the frequency decreases, the capacitive impedance is increased as the capacitor of electrode surface layer is charged. Also, the changes in the impedance values (Z) between the curves increase and reach a maximum at 0.1 Hz. At frequencies less than 0.1 Hz, the low frequency noise in the modifier is very high, which causes the impedance signal to fluctuate and make results unreliable.[32] The changes in impedance amplitude were plotted against the logarithmic concentration of the complementary HBV strands at 0.1 Hz. As can be seen, the amplitude of the impedance increases by increasing the concentration of the target strand, according to eq 3.

$$\Delta Z\ (\mathrm{k\Omega}) = 4599.7 \log C\ (\mathrm{M}) + 72822\ (R^2 = 0.9894) \quad (3)$$

The minimum detectable concentration (LOQ), 10 fM, is equivalent to 10^9 copies/mL of this HBV target sequence and can claim that the proposed method can be applied for identification of HBV DNA levels in the serum of patients before seroconversion.[33]

Table 1 briefly compares the characteristic performance of the present work with other previous reports for the electrochemical determination of HBV DNA. A significant sensitivity and low detection limit for the target DNA highlight the advantage of the proposed biosensor. In addition, the simplicity of this method, without using expensive, complex, and time-consuming label techniques and incorporating an external redox probe, makes it more interesting in the field of biosensing. Moreover, contamination of biological interface and surface samples by an outer indicator create unwanted interference in DNA detection, which can be avoided in the proposed method. In this regard, the use of an intrinsic surface probe as a hybridization indicator can be cited as the unique advantage of the fabricated biosensor.

Moreover, the reported biosensors based on using an inherent redox peak of the surface confined modifiers, as a characteristic peak for monitoring some biological, are indexed in Table S3. Compared to previous reports, the proposed modifying layer provides comparable advantages, such as low detection limit and the appropriate concentration range, which makes it suitable for analyzing various target biomolecules.

Evaluation of Selectivity and Reproducibility of DNA/Au/HCS-PANI/GCE. Selectivity is one of the most important benefits of using biological molecules as a recognition layer in biosensors. The evaluation of the selectivity of the proposed biosensor was assayed using different types of DNA strands, including a noncomplementary strand and a mutated one, in a concentration of 100 pM of the target DNA. As it is obvious in Figure S4, the tendency of the probe DNA to the complementary strand is significantly more favored than the mutated one.

The inter- and intra-assay were performed to estimate the repeatability and reproducibility of the biosensing system. Four biosensors were prepared independently to detect the target DNA with a concentration of 100 pM. The relative standard deviation (RSD) for these four parallel-prepared biosensors was 6.6%. Each biosensor was measured repetitively six times, and an RSD of 1.37% was achieved. These results provided an acceptable performance of the modifier and the developed method in the presented measurements.

Bioassay Application in Real Samples. Biomedical usability of a biosensor in real samples compared to the buffered media, without reducing its efficiency, is an important

DOI: 10.1021/acsbiomaterials.8b01520
ACS Biomater. Sci. Eng. 2019, 5, 2587−2594

factor in the clinical field. In this regard, the biosensor was examined in an 1% solution of human blood plasma without any additional processing steps and in the presence of the selected concentrations of the complementary HBV sequence. As seen in the inset of Figure S5A, the intrinsic electrochemical response of the modifier at the surface of Au/HCS-PANI/GCE, under the optimum temperature and after being exposed to 1% plasma solution for 90 min, shows a slight change, which refers to the stability of the response in this complex media. Also, measurement of the different concentrations of the HBV DNA complementary strands (from 0.1 pM to 1 nM) offers comparable sensitivity (eq 4), with the calibration curve in pure buffer solution (without any interfering agents) (Figure S5B).

$$\Delta I = 0.618 \log C\ (\mathrm{M}) + 11.54\ (R^2 = 0.9848) \quad (4)$$

CONCLUSION

In this study, the construction of an efficient and highly effective electrochemical biosensor composed of the biocompatible nanocomposite materials, Au/HCS-PANI, was introduced and applied for a sensitive detection of the HBV DNA marker. Owing to the high efficiency of electron transfer and high surface area of the proposed modifier for DNA detection, and based on the effect of the DNA immobilization and hybridization on the characteristic peak of PANI, a biosensor with high sensitivity, selectivity, and acceptable reproducibility was presented. Also, the evaluation of the proposed method showed that this biosensor has high capability for being used in complex biological matrices and can be used as an acceptable method for the detection of cancer-related biomolecules.

ASSOCIATED CONTENT

Supporting Information

The Supporting Information is available free of charge on the ACS Publications website at DOI: 10.1021/acsbiomaterials.8b01520.

CVs of modified electrodes at different scan rates of potential, electrochemical investigation of Au/HCS-PANI/GCE in the presence of ssDNA, optimization of parameters, selectivity, real sample investigation, table of the calculated active microscopic surface area for various type of electrodes, table of the R_{ct} and R_s parameters of the Au/HCS-PANI/GC electrode in the DNA modification steps, and table of the reported electrochemical biosensors based on the inherent peak of the modifier (PDF)

AUTHOR INFORMATION

Corresponding Author

*Tel/Fax: +98 2166165359; E-mail: shahrokhian@sharif.edu.

ORCID

Saeed Shahrokhian: 0000-0003-3138-6578

Notes

The authors declare no competing financial interest.

ACKNOWLEDGMENTS

The authors gratefully acknowledge the support of this work by the Research Council and the Center of Excellence for Nanostructures of the Sharif University of Technology, Tehran, Iran.

REFERENCES

(1) He, Q. Y.; Lau, G. K.; Zhou, Y.; Yuen, S. T.; Lin, M. C.; Kung, H. F.; Chiu, J. F. Serum biomarkers of hepatitis B virus infected liver inflammation: a proteomic study. *Proteomics* **2003**, *3* (5), 666−674.

(2) Liu, Y.-P.; Yao, C.-Y. Rapid and quantitative detection of hepatitis B virus. *World J. Gastroenterol.* **2015**, *21* (42), 11954.

(3) *Hepatitis B (chronic): Diagnosis and management of chronic hepatitis B in children, young people, and adults*; National Institute for Health and Care Excellence London, 2013.

(4) Brechot, C.; Scotto, J.; Charnay, P.; Hadchouel, M.; Degos, F.; Trepo, C.; Tiollais, P. Detection of hepatitis B virus DNA in liver and serum: a direct appraisal of the chronic carrier state. *Lancet* **1981**, *318* (8250), 765−768.

(5) Taleat, Z.; Khoshroo, A.; Mazloum-Ardakani, M. Screen-printed electrodes for biosensing: a review (2008−2013). *Microchim. Acta* **2014**, *181* (9−10), 865−891.

(6) Amiri, M.; Bezaatpour, A.; Jafari, H.; Boukherroub, R.; Szunerits, S. J. A. s. Electrochemical methodologies for the detection of pathogens. *ACS Sens.* **2018**, *3* (6), 1069−1086.

(7) Maity, D.; Kumar, R. T. R. J. A. s. Polyaniline anchored MWCNTs on fabric for high performance wearable ammonia sensor. *ACS Sens.* **2018**, *3* (9), 1822−1830.

(8) Peng, H.; Zhang, L.; Soeller, C.; Travas-Sejdic, J. J. B. Conducting polymers for electrochemical DNA sensing. *Biomaterials* **2009**, *30* (11), 2132−2148.

(9) Dhand, C.; Arya, S. K.; Datta, M.; Malhotra, B. Polyaniline−carbon nanotube composite film for cholesterol biosensor. *Anal. Biochem.* **2008**, *383* (2), 194−199.

(10) Karyakin, A.; Strakhova, A.; Yatsimirsky, A. Self-doped polyanilines electrochemically active in neutral and basic aqueous solutions.: Electropolymerization of substituted anilines. *J. Electroanal. Chem.* **1994**, *371* (1−2), 259−265.

(11) Bartlett, P. N.; Simon, E. Poly (aniline)−poly (acrylate) composite films as modified electrodes for the oxidation of NADH. *Phys. Chem. Chem. Phys.* **2000**, *2* (11), 2599−2606.

(12) Tian, S.; Liu, J.; Zhu, T.; Knoll, W. Polyaniline doped with modified gold nanoparticles and its electrochemical properties in neutral aqueous solution. *Chem. Commun.* **2003**, No. 21, 2738−2739.

(13) Granot, E.; Basnar, B.; Cheglakov, Z.; Katz, E.; Willner, I. Enhanced bioelectrocatalysis using single-walled carbon nanotubes (SWCNTs)/polyaniline hybrid systems in thin-film and microrod structures associated with electrodes. *Electroanalysis* **2006**, *18* (1), 26−34.

(14) Yang, C.; Denno, M. E.; Pyakurel, P.; Venton, B. J. Recent trends in carbon nanomaterial-based electrochemical sensors for biomolecules: A review. *Anal. Chim. Acta* **2015**, *887*, 17−37.

(15) Bagheri, S.; Termehyousefi, A.; Mansouri, N.; Amani Babadi, A.; Abd Karim, M. S.; Adib Kadri, N. Carbon-Based Nanobiohybrid Thin Film for Amperometric Glucose Sensing. *ACS Biomater. Sci. Eng.* **2017**, *3* (9), 2059−2063.

(16) Ghosal, K.; Sarkar, K. J. A. B. S. Biomedical applications of graphene nanomaterials and beyond. *ACS Biomater. Sci. Eng.* **2018**, *4* (8), 2653−2703.

(17) Li, S.; Pasc, A.; Fierro, V.; Celzard, A. Hollow carbon spheres, synthesis and applications−a review. *J. Mater. Chem. A* **2016**, *4* (33), 12686−12713.

(18) Wang, X.; Feng, J.; Bai, Y.; Zhang, Q.; Yin, Y. Synthesis, properties, and applications of hollow micro-/nanostructures. *Chem. Rev.* **2016**, *116* (18), 10983−11060.

(19) Liu, R.; Mahurin, S. M.; Li, C.; Unocic, R. R.; Idrobo, J. C.; Gao, H.; Pennycook, S. J.; Dai, S. Dopamine as a carbon source: the controlled synthesis of hollow carbon spheres and yolk-structured carbon nanocomposites. *Angew. Chem., Int. Ed.* **2011**, *50* (30), 6799−6802.

(20) Bo, Y.; Yang, H.; Hu, Y.; Yao, T.; Huang, S. A novel electrochemical DNA biosensor based on graphene and polyaniline nanowires. *Electrochim. Acta* **2011**, *56* (6), 2676−2681.

(21) Hui, N.; Sun, X.; Niu, S.; Luo, X. PEGylated polyaniline nanofibers: antifouling and conducting biomaterial for electro-

DOI: 10.1021/acsbiomaterials.8b01520
ACS Biomater. Sci. Eng. 2019, 5, 2587−2594

chemical DNA sensing. *ACS Appl. Mater. Interfaces* **2017**, *9* (3), 2914−2923.
(22) Zhu, Q.; Gao, F.; Yang, Y.; Zhang, B.; Wang, W.; Hu, Z.; Wang, Q. Electrochemical preparation of polyaniline capped Bi2S3 nanocomposite and its application in impedimetric DNA biosensor. *Sens. Actuators, B* **2015**, *207*, 819−826.
(23) Shoaie, N.; Forouzandeh, M.; Omidfar, K. Voltammetric determination of the Escherichia coli DNA using a screen-printed carbon electrode modified with polyaniline and gold nanoparticles. *Microchim. Acta* **2018**, *185* (4), 217.
(24) Du, M.; Yang, T.; Li, X.; Jiao, K. Fabrication of DNA/graphene/polyaniline nanocomplex for label-free voltammetric detection of DNA hybridization. *Talanta* **2012**, *88*, 439−444.
(25) Wang, L.; Hua, E.; Liang, M.; Ma, C.; Liu, Z.; Sheng, S.; Liu, M.; Xie, G.; Feng, W. Graphene sheets, polyaniline and AuNPs based DNA sensor for electrochemical determination of BCR/ABL fusion gene with functional hairpin probe. *Biosens. Bioelectron.* **2014**, *51*, 201−207.
(26) Stöber, W.; Fink, A.; Bohn, E. Controlled growth of monodisperse silica spheres in the micron size range. *J. Colloid Interface Sci.* **1968**, *26* (1), 62−69.
(27) Noonan, O.; Zhang, H.; Song, H.; Xu, C.; Huang, X.; Yu, C. In situ Stöber templating: facile synthesis of hollow mesoporous carbon spheres from silica−polymer composites for ultra-high level in-cavity adsorption. *J. Mater. Chem. A* **2016**, *4* (23), 9063−9071.
(28) Lei, Z.; Chen, Z.; Zhao, X. Growth of polyaniline on hollow carbon spheres for enhancing electrocapacitance. *J. Phys. Chem. C* **2010**, *114* (46), 19867−19874.
(29) Moulton, S.; Innis, P.; Kane-Maguire, L.; Ngamna, O.; Wallace, G. Polymerisation and characterisation of conducting polyaniline nanoparticle dispersions. *Curr. Appl. Phys.* **2004**, *4* (2−4), 402−406.
(30) Song, E.; Choi, J.-W. Conducting polyaniline nanowire and its applications in chemiresistive sensing. *Nanomaterials* **2013**, *3* (3), 498−523.
(31) Jarczewska, M.; Kékedy-Nagy, L.; Nielsen, J. S.; Campos, R.; Kjems, J.; Malinowska, E.; Ferapontova, E. E. Electroanalysis of pM-levels of urokinase plasminogen activator in serum by phosphorothioated RNA aptamer. *Analyst* **2015**, *140* (11), 3794−3802.
(32) Ye, W.; Guo, J.; Chen, S.; Yang, M. Nanoporous membrane based impedance sensors to detect the enzymatic activity of botulinum neurotoxin A. *J. Mater. Chem. B* **2013**, *1* (47), 6544−6550.
(33) Chen, C. J.; Yang, H. I.; Iloeje, U. H. Hepatitis B virus DNA levels and outcomes in chronic hepatitis B. *Hepatology* **2009**, *49* (S5), S72.
(34) Shakoori, Z.; Salimian, S.; Kharrazi, S.; Adabi, M.; Saber, R. Electrochemical DNA biosensor based on gold nanorods for detecting hepatitis B virus. *Anal. Bioanal. Chem.* **2015**, *407* (2), 455−461.
(35) Xiang, Q.; Huang, J.; Huang, H.; Mao, W.; Ye, Z. A label-free electrochemical platform for the highly sensitive detection of hepatitis B virus DNA using graphene quantum dots. *RSC Adv.* **2018**, *8* (4), 1820−1825.
(36) Li, X.; Scida, K.; Crooks, R. M. Detection of hepatitis B virus DNA with a paper electrochemical sensor. *Anal. Chem.* **2015**, *87* (17), 9009−9015.
(37) Mashhadizadeh, M. H.; Talemi, R. P. Synergistic effect of magnetite and gold nanoparticles onto the response of a label-free impedimetric hepatitis B virus DNA biosensor. *Mater. Sci. Eng., C* **2016**, *59*, 773−781.
(38) Shi, L.; Yu, Y.; Chen, Z.; Zhang, L.; He, S.; Shi, Q.; Yang, H. A label-free hemin/G-quadruplex DNAzyme biosensor developed on electrochemically modified electrodes r detection of a HBV DNA segment. *RSC Adv.* **2015**, *5* (15), 11541−11548.
(39) Zheng, J.; Chen, C.; Wang, X.; Zhang, F.; He, P. A sequence-specific DNA sensor for Hepatitis B virus diagnostics based on the host−guest recognition. *Sens. Actuators, B* **2014**, *199*, 168−174.
(40) Li, F.; Xu, Y.; Yu, X.; Yu, Z.; He, X.; Ji, H.; Dong, J.; Song, Y.; Yan, H.; Zhang, G. A "signal on" protection-displacement-hybridization-based electrochemical hepatitis B virus gene sequence sensor with high sensitivity and peculiar adjustable specificity. *Biosens. Bioelectron.* **2016**, *82*, 212−216.
(41) Eksin, E.; Erdem, A. Chitosan-carbon Nanofiber Modified Single-use Graphite Electrodes Developed for Electrochemical Detection of DNA Hybridization Related to Hepatitis B Virus. *Electroanalysis* **2016**, *28* (10), 2514−2521.
(42) Gao, N.; Gao, F.; He, S.; Zhu, Q.; Huang, J.; Tanaka, H.; Wang, Q. Graphene oxide directed in-situ deposition of electroactive silver nanoparticles and its electrochemical sensing application for DNA analysis. *Anal. Chim. Acta* **2017**, *951*, 58−67.
(43) Huang, S.; Feng, M.; Li, J.; Liu, Y.; Xiao, Q. Voltammetric determination of attomolar levels of a sequence derived from the genom of hepatitis B virus by using molecular beacon mediated circular strand displacement and rolling circle amplification. *Microchim. Acta* **2018**, *185* (3), 206.
(44) Wang, S.; Li, L.; Jin, H.; Yang, T.; Bao, W.; Huang, S.; Wang, J. Electrochemical detection of hepatitis B and papilloma virus DNAs using SWCNT array coated with gold nanoparticles. *Biosens. Bioelectron.* **2013**, *41*, 205−210.
(45) Chen, J.; Weng, S.; Chen, Q.; Liu, A.; Wang, F.; Chen, J.; Yi, Q.; Liu, Q.; Lin, X. Development of an Electrochemical Sensing Technique for Rapid Genotyping of Hepatitis B Virus. *Sensors* **2014**, *14* (3), 5611−5621.
(46) Nie, G.; Bai, Z.; Chen, J.; Yu, W. Simple label-free femtomolar DNA detection based on a nanostructure composite material: MWNT-doped poly (indole-6-carboxylic acid). *ACS Macro Lett.* **2012**, *1* (11), 1304−1307.
(47) Han, X.; Fang, X.; Shi, A.; Wang, J.; Zhang, Y. An electrochemical DNA biosensor based on gold nanorods decorated graphene oxide sheets for sensing platform. *Anal. Biochem.* **2013**, *443* (2), 117−123.

DOI: 10.1021/acsbiomaterials.8b01520
ACS Biomater. Sci. Eng. 2019, 5, 2587−2594